JOURNAL OF COMPUTATIONAL PHYSICS 117, 240–250 (1995)

A Second-Order Description of Shock Structure

J. M. REESE AND L. C. WOODS

Mathematical Institute, University of Oxford, 24-29 St. Giles, Oxford OX1 3LB, United Kingdom

F. J. P. THIVET

Centre d'Etudes et de Recherches de Toulouse, ONERA, Département d'Aérothermodynamique BP 4025, 31055 Toulouse Cedex, France

AND

S. M. CANDEL

Laboratoire d'Energétique Moléculaire et Macroscopique, Combustion, UPR 288 CNRS, Ecole Centrale Paris, 92295 Châtenay-Malabry, France

Received May 3, 1993; revised November 3, 1993

The structure of gas-dynamic shock waves is of interest in hypersonic flow studies and also constitutes a straightforward test for competing kinetic theories. The description of the shock profiles may be obtained from a second-order theory in the Knudsen number. The BGK approximation to the Boltzmann equation introduces additional terms in the transport of momentum and energy. These relations, known as the Burnett equations, improve the agreement between calculated shock profiles and experiment. However, for some formulations of these equations, the solution breaks down at a critical Mach number. In addition, certain terms in the Burnett equations allow unphysical effects in gas flow. A modified kinetic theory has been proposed by Woods (*An Introduction to the Kinetic Theory of Gases and Magnetoplasmas*, Oxford Univ. Press, Oxford, 1993) which eliminates the frame dependence of the standard kinetic theory and corrects some of the second-order terms. This article describes a novel method devised to solve the time-independent conservation equations, including the second-order terms. The method is used to solve the shock structure problem in one dimension. It is based on a finite difference global scheme (FDGS), in which a Newton procedure is applied to a discretized version of the governing equations and boundary conditions. The method is first applied to the Navier–Stokes formulation of the shock equations. It is then successfully used to integrate a modified version of the second-order equations derived by Woods for monatomic gases, up to a Mach number of 30. Results of the calculations are compared with experimental data for Argon gas flows characterized by upstream Mach numbers up to 10. The agreement is good, well within the data point spread. The FDGS method converges rapidly and it may be used to study other problems of the same general nature.

1. INTRODUCTION

Shock wave structure is a subject of continuing interest. It is considered, for example, in the analysis of certain hypersonic flow situations. The problem is also studied to test second-order theories based on the Boltzmann equation. One such theory has been developed by Woods [2] to replace the Burnett equations. This new formulation is employed in this article to examine shock wave profiles, determine the shock wave thickness as a function of the Mach number, and compare this quantity with experimental measurements. The second-order shock wave equations are solved using an original finite difference global scheme, which relies on a discretized version of the governing equations and boundary conditions, and a global Newton iteration procedure. This approach is suggested by our experience in flame and reactive flow calculations (see, e.g., [3]), and it uses a scheme initially devised by Smooke [4]. However, the application to the shock structure problem is not as straightforward as it may seem. To devise a successful integration scheme, it is important to understand some of the peculiar features of the problem. This may be achieved by examining the shock wave structure with the Navier–Stokes equations. The Navier–Stokes formulation is known to yield incorrect shock profiles even at moderate Mach numbers, but it provides an excellent test problem. A phase plane analysis of this case provides guidelines for the discretization scheme adopted in the finite difference global solution method, designated from here on as the FDGS method. The Navier–Stokes shock structure is also used to check the present solution procedure. This is accomplished by first calculating the shock profiles with a more standard path integration in the phase plane and comparing these solutions with those obtained from the FDGS method.

The shock structure equations are presented in Section 2. A phase plane analysis of the Navier–Stokes shock structure is carried out in Section 3. The path integration scheme deduced

0021-9991/95 $6.00

from the phase plane analysis is briefly described in Section 4. The finite difference global solution method is then introduced in Section 5, and results obtained with the two integration schemes are compared in Section 6.1. Shock profiles obtained from a modified version of the second-order formulation derived by Woods are discussed and the shock thickness deduced in this case are determined as a function of the upstream Mach number (Section 6.2). A comparison with experimental measurements of shock wave thickness is then carried out.

2. SHOCK STRUCTURE EQUATIONS

2.1. *General Expression of the Second-Order Fluxes*

At each point in space and time, the state of a monatomic ideal gas flow is determined by the velocity $\mathbf{v}$, the temperature T, and the density ρ. The pressure p obeys the perfect gas law,

$$p = \rho RT, \tag{1}$$

where $R = k_b/m$ is the gas constant, k_b is the Boltzmann's constant, and m is the molecular mass. Specific heats at constant volume and pressure are denoted c_v and c_p, respectively. A monatomic ideal gas is characterized by

$$c_v = \tfrac{3}{2}R, \quad c_p = \tfrac{5}{2}R, \tag{2}$$

such that the isentropic constant γ, defined as the ratio of c_p to c_v, is equal to $\frac{5}{3}$. The speed of sound c is given in the medium by the simple relation

$$c^2 = \gamma \frac{p}{\rho}. \tag{3}$$

The conservation equations for momentum and energy include a viscous stress tensor $\mathbf{\Pi}$ and a heat flux vector $\mathbf{Q}$. These transport terms may be obtained through the classical Chapman–Enskog expansion in Knudsen number of the Boltzmann equation:

$$\mathbf{\Pi} = \mathbf{\Pi}^{(0)} + \mathbf{\Pi}^{(1)} + \mathbf{\Pi}^{(2)} + \ldots, \tag{4a}$$

$$\mathbf{Q} = \mathbf{Q}^{(0)} + \mathbf{Q}^{(1)} + \mathbf{Q}^{(2)} + \ldots. \tag{4b}$$

At zeroth order, this procedure gives

$$\mathbf{\Pi}^{(0)} = \mathbf{0}, \tag{5a}$$

$$\mathbf{Q}^{(0)} = \mathbf{0}. \tag{5b}$$

Substituting these fluxes in the conservation equations gives the Euler equations.

The next approximation gives

$$\mathbf{\Pi}^{(1)} = -2\mu \mathring{\mathbf{e}}, \tag{6a}$$

$$\mathbf{Q}^{(1)} = -k \nabla T, \tag{6b}$$

where $\mathring{\mathbf{e}} \equiv \mathbf{e} - \frac{1}{3}\mathrm{tr}(\mathbf{e})\mathbf{1}$, $\mathbf{e} = \frac{1}{2}(\nabla \mathbf{v} + {}^t\nabla \mathbf{v})$, and μ and k are, respectively, the viscosity and the heat conductivity of the gas. For a monatomic gas modeled by point centers of force, the kinetic theory leads to a viscosity proportional to T^s and the Prandtl number $\mathrm{Pr} = \mu c_p/k$ is a constant equal to $\frac{2}{3}$. The temperature exponent s is given by

$$s = \frac{1}{2} + \frac{2}{\nu - 1}, \tag{7}$$

where ν is the power index of the inter-molecular force law. For argon gas at NTP, $\nu = 7.5$ is cited by Chapman and Cowling [1] based on early viscosity data. Recent work by Lumpkin and Chapman [5] suggests that $\nu = 9.0$ is a better approximation, which is confirmed through systematic calculation of shock wave profiles. The conservation equations, together with the fluxes (6), define the Navier–Stokes equations.

At second-order, the classical BGK expansion of the Boltzmann equation leads to the accepted form of the Burnett equations:

$$\mathbf{\Pi}_B^{(2)} = \frac{\mu^2}{p}\Big[\tilde{\omega}_1 \nabla \cdot \mathbf{v}\mathring{\mathbf{e}} + \tilde{\omega}_2 (D\mathring{\mathbf{e}} - 2\,\overset{\circ}{\overline{\nabla \mathbf{v}}}\mathring{\mathbf{e}}) + \tilde{\omega}_3 R\,\overset{\circ}{\overline{\nabla\nabla T}} + \frac{\tilde{\omega}_4}{\rho T}\overset{\circ}{\overline{\nabla p\,\nabla T}} + \tilde{\omega}_5 \frac{R}{T}\overset{\circ}{\overline{\nabla T \nabla T}} + \tilde{\omega}_6 \overset{\circ}{\overline{\mathring{\mathbf{e}} \cdot \mathring{\mathbf{e}}}}\Big], \tag{8a}$$

$$\mathbf{Q}_B^{(2)} = R\frac{\mu^2}{p}\Big[\theta_1 \nabla \cdot \mathbf{v}\nabla T + \theta_2 (D\nabla T - \nabla \mathbf{v} \cdot \nabla T) + \theta_3 \frac{T}{p}\nabla p \cdot \mathring{\mathbf{e}} + \theta_4 T \nabla \cdot \mathring{\mathbf{e}} + 3\theta_5 \nabla T \cdot \mathring{\mathbf{e}}\Big], \tag{8b}$$

where D is the convective derivative, and the constant coefficients are:

$$\tilde{\omega}_1 = \tfrac{4}{3}(\tfrac{7}{2} - s),\ \tilde{\omega}_2 = 2,\ \tilde{\omega}_3 = 3,\quad \tilde{\omega}_4 = 0,\ \tilde{\omega}_5 = 3s,\ \tilde{\omega}_6 = 8,$$
$$\theta_1 = \tfrac{15}{4}(\tfrac{7}{2} - s),\ \theta_2 = \tfrac{45}{8},\ \theta_3 = -3,\ \theta_4 = 3,\ \theta_5 = \tfrac{35}{4} + s. \tag{9}$$

In order to determine the shock wave structure in one dimension, Lumpkin and Chapman [5] solve the full time-dependent conservation equations subject to the Rankine–Hugoniot jump conditions satisfied at each end. They iterate the hyperbolic

flow equations using a modified MacCormack method until a steady state is reached and there is no further change in the shock profile. As Zhong *et al.* [6] showed, the Burnett equations applied in this manner are unstable to small oscillations in the solution. The problem is solved by augmenting the Burnett equations with selected third-order terms until a stable solution can be shown to exist. The shock thickness values obtained for argon show reasonable agreement with experiment; however, the full third-order equations ("super-Burnett") are unstable in the same way as the Burnett equations. Numerical convergence can only be assured by including additional higher-order terms, although the exact form of these extra terms is still under investigation (see, e.g., [7]).

Woods [2] has suggested that the second-order terms derive from an inappropriate frame-dependent formulation of the BGK expansion. Inconsistencies become apparent when the accepted form of the Burnett equations is examined more closely. One finds that some of these second-order terms are consequences of not properly distinguishing between convection and diffusion. This failure arises in the initial formulation of the kinetic equation describing the evolution of the velocity distribution function, not in its expansion method of solution. Diffusion is due to molecular agitation superimposed on a reference frame that not only has the speed of the fluid element, but which also accelerates and spins with it. Spurious terms in the Burnett equations arise because standard kinetic theories, like those due to Boltzmann and Fokker–Planck, ignore fluid accelerations. These theories are valid only to first-order in Knudsen number. As an example of the "spurious terms," the expression (8b) indicates that even in the absence of temperature gradients, heat flux can be generated through fluid shear alone; this appears to have no physical justification.

A new approach to kinetic theory has been developed by Woods [2]. By incorporating fluid accelerations, it eliminates convective terms from the second-order transport equations, and the viscous stress and heat flux become

$$\mathbf{\Pi}_W^{(2)} = \frac{\mu^2}{p}\left[\tilde{\omega}_1 \nabla\cdot\mathbf{v}\mathring{\mathbf{e}} + \tilde{\omega}_3 R \overset{\circ}{\overline{\nabla\nabla T}} + \tilde{\omega}_5 \frac{R}{T}\overset{\circ}{\overline{\nabla T\,\nabla T}} + \tilde{\omega}_6 \overset{\circ}{\overline{\mathring{\mathbf{e}}\cdot\mathring{\mathbf{e}}}}\right], \tag{10a}$$

$$\mathbf{Q}_W^{(2)} = R\frac{\mu^2}{p}[\theta_1 \nabla\cdot\mathbf{v}\,\nabla T + \theta_2(D\,\nabla T - \mathbf{\Omega}\times\nabla T) + 3\theta_5\,\nabla T\cdot\mathring{\mathbf{e}}], \tag{10b}$$

where $\mathbf{\Omega} \equiv \frac{1}{2}\nabla\times\mathbf{v}$, the fluid spin, and where the constants are

$$\begin{aligned} &\tilde{\omega}_1 = \tfrac{4}{3}(4-s), \quad \tilde{\omega}_3 = 3, \quad \tilde{\omega}_5 = 3s, \quad \tilde{\omega}_6 = 6, \\ &\theta_1 = \tfrac{15}{4}(\tfrac{9}{2}-s), \quad \theta_2 = \tfrac{45}{4}, \quad \theta_5 = \tfrac{35}{4}+s. \end{aligned} \tag{11}$$

2.2. *The One-Dimensional Problem*

Consider a planar stationary shock wave established in the one-dimensional flow of a monatomic gas between supersonic upstream conditions (subscript 1) and downstream conditions (subscript 2). The one-dimensional flow of the gas is governed by the conservation equations

$$\rho u = m_0, \tag{12a}$$

$$p + \rho u^2 + \pi = p_0, \tag{12b}$$

$$\rho u\left(c_p T + \frac{u^2}{2}\right) + u\pi + q = m_0 h_0, \tag{12c}$$

where m_0 is the mass flow rate, p_0 is the stagnation pressure, h_0 is the stagnation specific enthalpy, and where π and q are the components of the stress tensor and of the heat flux in the flow direction x. Using Eq. (12a) and the perfect gas law (1), this set of equations reduces to

$$-\frac{u}{m_0}\pi = RT + u^2 - \frac{p_0}{m_0}u, \tag{13a}$$

$$-\frac{1}{m_0}q = c_v T - \frac{u^2}{2} + \frac{p_0}{m_0}u - h_0. \tag{13b}$$

The Navier–Stokes transport terms become, in one dimension,

$$\pi^{(1)} = -\frac{4}{3}\mu\frac{du}{dx}, \tag{14a}$$

$$q^{(1)} = -k\frac{dT}{dx}. \tag{14b}$$

In the second-order terms, even when the flow is unsteady, the time derivatives may be eliminated using the zeroth order equalities arising in the conservation equations:

$$\rho D\mathbf{v} = -\nabla p, \tag{15a}$$

$$DT = -(\gamma-1)T\nabla\cdot\mathbf{v}. \tag{15b}$$

Substituting for the convective derivative from Eqs. (15), we obtain the one dimensional expressions of the second-order fluxes, as used by Lumpkin and Chapman [5],

$$\begin{aligned} \pi_B^{(2)} = \frac{2}{3}\frac{\mu^2}{p}\Bigg[&\left(\tilde{\omega}_1 - \frac{7}{3}\tilde{\omega}_2 + \frac{1}{3}\tilde{\omega}_6\right)\left(\frac{\partial u}{\partial x}\right)^2 \\ &- (\tilde{\omega}_2 - \tilde{\omega}_3)R\frac{\partial^2 T}{\partial x^2} - (\tilde{\omega}_2 - \tilde{\omega}_4)\frac{R}{\rho}\frac{\partial\rho}{\partial x}\frac{\partial T}{\partial x} \\ &+ (\tilde{\omega}_4 + \tilde{\omega}_5)\frac{R}{T}\left(\frac{\partial T}{\partial x}\right)^2 \\ &+ \tilde{\omega}_2\frac{RT}{\rho^2}\left(\frac{\partial\rho}{\partial x}\right)^2 - \tilde{\omega}_2\frac{RT}{\rho}\frac{\partial^2\rho}{\partial x^2}\Bigg], \end{aligned} \tag{16a}$$

$$q_B^{(2)} = R\frac{\mu^2}{p}\left[\left(\theta_1 - \frac{8}{3}\theta_2 + \frac{2}{3}\theta_3 + 2\theta_5\right)\frac{\partial u}{\partial x}\frac{\partial T}{\partial x} - \frac{2}{3}(\theta_2 - \theta_4)\,T\frac{\partial^2 u}{\partial x^2} + \frac{2}{3}\theta_3\frac{T}{\rho}\frac{\partial \rho}{\partial x}\frac{\partial u}{\partial x}\right], \tag{16b}$$

while the expressions derived from Woods' formulation can be written

$$\pi_W^{(2)} = \frac{2}{3}\frac{\mu^2}{p}\left[\left(\tilde{\omega}_1 + \frac{1}{3}\tilde{\omega}_6\right)\left(\frac{\partial u}{\partial x}\right)^2 + \tilde{\omega}_3 R\frac{\partial^2 T}{\partial x^2} + \tilde{\omega}_5\frac{R}{T}\left(\frac{\partial T}{\partial x}\right)^2\right], \tag{17a}$$

$$q_W^{(2)} = R\frac{\mu^2}{p}\left[\left(\theta_1 - \frac{5}{3}\theta_2 + 2\theta_5\right)\frac{\partial u}{\partial x}\frac{\partial T}{\partial x} - \frac{2}{3}\theta_2 T\frac{\partial^2 u}{\partial x^2}\right]. \tag{17b}$$

The exact definition of the convective derivative is $D \equiv \partial/\partial t + \mathbf{v}\cdot\nabla$, which would reduce to $D = u(d/dx)$ for steady one-dimensional flow. However, Welder and Chapman [7] point out that the Burnett equations are unstable if this exact definition is used. Through the Euler equations (15) or the Navier–Stokes equations, different expressions for the convective derivative acting on ∇T can be obtained. We use the zeroth order (Euler) formulation, as higher order forms introduce additional viscous terms into the overall second-order equations. This further complicates the system of equations to be solved and would not necessarily improve the accuracy of obtained solutions. For simplicity the zeroth order formulation is used, and this will be shown to give good results.

In what follows, the shock structure will be examined using the expressions (17) in combination with the basic conservation relations (13) and the first-order fluxes (14). It is interesting to note that the energy equation takes a form which is analogous to the Korteweg–de Vries equation. It is known that the KdV equation exhibits shock profiles modulated by oscillations (see, e.g., [8]). We would, therefore, expect the shock curves obtained through solution of these equations to show some mild oscillations. This will be discussed further in Section 6.2.

2.3. *The Non-Dimensional Equations*

It is convenient to replace the conservation equations by dimensionless forms. To this purpose we use the following minimal set of reference quantities: the speed of sound c_1, the pressure p_1, the heat at constant pressure c_{p1} and the viscosity μ_1.

One may then define a complete set of reduced variables,

$$u = c_1\bar{u}, \quad p = p_1\bar{p}, \quad \rho = \frac{p_1}{c_1^2}\bar{\rho}, \quad T = \frac{c_1^2}{R}\bar{T}, \quad \mu = \mu_1\bar{\mu}, \quad k = \frac{\mu_1 c_{p1}}{\mathrm{Pr}}\bar{\mu}, \quad x = \lambda_1\bar{x}, \tag{18}$$

where the upstream mean free path λ_1 is used as a reference length-scale. A suitable measure of λ_1 is

$$\lambda_1 = \frac{\mu_1}{p_1}\sqrt{2RT_1}, \tag{19}$$

which is close to the standard Maxwellian definition of mean free path. This may also be expressed as a function of the reference quantities:

$$\lambda_1 = \frac{\mu_1 c_1}{p_1}\sqrt{2/\gamma}, \tag{20}$$

With these notations the fluxes become

$$\pi = \sqrt{\gamma/2}\,p_1\bar{\pi}, \tag{21a}$$

$$q = \frac{\gamma}{\gamma - 1}\frac{c_1 p_1}{\mathrm{Pr}}\sqrt{\gamma/2}\,\bar{q}, \tag{21b}$$

with

$$\bar{\pi} = -\frac{4}{3}\bar{\mu}\frac{d\bar{u}}{d\bar{x}} + \frac{2}{3}\frac{\bar{\mu}^2}{M_1\sqrt{2\gamma}}\frac{\bar{u}}{\bar{T}}\left[\left(\tilde{\omega}_1 + \frac{1}{3}\tilde{\omega}_6\right)\left(\frac{d\bar{u}}{d\bar{x}}\right)^2 + \tilde{\omega}_3\frac{d^2\bar{T}}{d\bar{x}^2} + \frac{\tilde{\omega}_5}{\bar{T}}\left(\frac{d\bar{T}}{d\bar{x}}\right)^2\right], \tag{22a}$$

$$\bar{q} = -\bar{\mu}\frac{d\bar{T}}{d\bar{x}} + \frac{\gamma - 1}{\gamma}\frac{\mathrm{Pr}\,\bar{\mu}^2}{M_1\sqrt{2\gamma}}\frac{\bar{u}}{\bar{T}}\left[\left(\theta_1 - \frac{5}{3}\theta_2 + 2\theta_5\right)\frac{d\bar{u}}{d\bar{x}}\frac{d\bar{T}}{d\bar{x}} - \frac{2}{3}\theta_2\bar{T}\frac{d^2\bar{u}}{d\bar{x}^2}\right]. \tag{22b}$$

Introducing these expressions into the reduced set of Eqs. (13), we obtain

$$-\frac{1}{M_1\sqrt{2\gamma}}\bar{u}\,\bar{\pi} = \bar{T} + \bar{u}^2 - \tilde{p}_0\bar{u}, \tag{23a}$$

$$-\frac{1}{\mathrm{Pr}\,M_1}\sqrt{\frac{\gamma}{2}}\,\bar{q} = \bar{T} - \frac{\gamma - 1}{2}\bar{u}^2 + (\gamma - 1)\tilde{p}_0\bar{u} - \tilde{h}_0, \tag{23b}$$

where the upstream Mach number $M_1 = u_1/c_1$ and where

$$\tilde{p}_0 = \frac{1}{\gamma M_1}(1 + \gamma M_1^2), \tag{24a}$$

$$\tilde{h}_0 = 1 + \frac{\gamma - 1}{2}M_1^2. \tag{24b}$$

3. PHASE PLANE ANALYSIS OF THE NAVIER–STOKES EQUATIONS

To understand the specific difficulties of the shock structure problem, it is worth examining the shock equations in the phase

plane. Such an analysis was conducted in the early work of Ludford [9], and an excellent synthesis of the main results is presented by Hayes [10]. The purpose of this section is to supply the conclusions which are useful in the numerical solution of the present problem.

3.1. *The General Solution*

When considering the first-order expressions of the fluxes (6), the system (23) becomes

$$\frac{4}{3M_1\sqrt{2\gamma}}\bar{u}\,\bar{\mu}\frac{d\bar{u}}{d\bar{x}} = \bar{T} + \bar{u}^2 - \tilde{p}_0\bar{u}, \tag{25a}$$

$$\frac{1}{\mathrm{Pr}\,M_1}\sqrt{\gamma/2}\,\bar{\mu}\frac{d\bar{T}}{d\bar{x}} = \bar{T} - \frac{\gamma-1}{2}\bar{u}^2 + (\gamma-1)\tilde{p}_0\bar{u} - \tilde{h}_0. \tag{25b}$$

Hence the monotonic solutions of system (25) are also solutions of the equation:

$$\frac{d\bar{T}}{d\bar{u}} = \frac{4\,\mathrm{Pr}}{3\gamma}\bar{u}\frac{g(\bar{u},\bar{T})}{f(\bar{u},\bar{T})}, \tag{26}$$

where $f(\bar{u},\bar{T})$ and $g(\bar{u},\bar{T})$ are the right-hand sides of Eqs. (25a) and (25b), respectively. In the phase plane $(\bar{u},\bar{T})$, the solutions of system (25) are connected by integral curves given by the first-order differential equation (26). The spatial evolution may be retrieved by the integration of equation (25a):

$$\frac{d\bar{x}}{d\bar{u}} = \frac{4}{3M_1\sqrt{2\gamma}}\frac{\bar{\mu}\,\bar{u}}{f(\bar{u},\bar{T})}. \tag{27}$$

However, the upstream and downstream states are stationary points of the system (25) because

$$f(\bar{u}_i,\bar{T}_i) = 0, \quad g(\bar{u}_i,\bar{T}_i) = 0 \quad \forall i = 1,2, \tag{28}$$

and Eqs. (26) or (27) cannot be used to start the integration process. Thus any marching integration scheme must be initialized by an expansion of Eqs. (25) around one of the states 1 or 2. Introducing perturbations of the stationary states:

$$\bar{u} = \bar{u}_i + \delta\bar{u}, \quad \bar{T} = \bar{T}_i + \delta\bar{T}, \tag{29}$$

and looking for exponential solutions of the form $\exp\{\kappa_i(3M_1\sqrt{2\gamma}/4\bar{\mu}_i)\bar{x}\}$, we obtain a linear homogeneous system:

$$\delta\bar{T} + [(2-\kappa_i)\bar{u}_i - \tilde{p}_0]\,\delta\bar{u} = 0, \tag{30a}$$

$$\left(1 - \frac{3\gamma}{4\,\mathrm{Pr}}\kappa_i\right)\delta\bar{T} - (\gamma-1)(\bar{u}_i - \tilde{p}_0)\,\delta\bar{u} = 0. \tag{30b}$$

This system has non-trivial solutions if and only if κ_i is equal to one of the two values

$$\kappa_i^{\pm} = \frac{-b_i \pm \sqrt{b_i^2 - 4a_ic_i}}{2a_i}, \tag{31}$$

with

$$a_i = \frac{3}{4}\frac{\gamma}{\mathrm{Pr}}\bar{u}_i, \tag{32a}$$

$$b_i = -\left[\frac{3\gamma}{4\,\mathrm{Pr}}(2\bar{u}_i - \tilde{p}_0) + \bar{u}_i\right], \tag{32b}$$

$$c_i = (\gamma+1)\bar{u}_i - \gamma\tilde{p}_0. \tag{32c}$$

In order to determine the sign of $\kappa_i^{\pm}$, we may use the following relations:

$$a_i > 0, \tag{33a}$$

$$-b_1 = \left[\left(\frac{3\gamma}{4\,\mathrm{Pr}} + 1\right)M_1 - \frac{1}{\gamma M_1}\right] > 0, \tag{33b}$$

$$c_1 = -c_2 = \frac{M_1^2 - 1}{M_1} > 0. \tag{33c}$$

Under these conditions $\kappa_1^{\pm} > 0$, $\kappa_2^- < 0$, and $\kappa_2^+ > 0$. This indicates that the upstream point is an unstable node and the downstream point is a saddle point. Consequently, any integration method must begin with the only stable solution of the problem; starting from downstream in a direction defined by the eigenvector $(\delta\bar{u}, \delta\bar{T})^t$ corresponding to the negative eigenvalue κ_2^- of the system (30). The components of this eigenvector are then related by

$$\delta\bar{T} = -[(2-\kappa_2^-)\bar{u}_2 - \tilde{p}_0]\,\delta\bar{u}. \tag{34}$$

3.2. *The Non-conductive Solution*

The general solutions corresponding to finite Prandtl numbers are limited by two particular cases. One of them is the non-conductive case, for which the Prandtl number is infinite. Equation (25b) degenerates into an algebraic relation which gives the temperature directly as a function of the velocity. Equation (27) is still valid and describes the spatial evolution of the variables.

3.3. *The Non-viscous Solution*

This is the other limit for the general solution. Since the upstream viscosity cannot be used as a reference quantity, it may be replaced by an expression involving the conductivity,

$2k_1/3c_{p1}$, such that the mean free path is now given by

$$\lambda_1 = \frac{2}{3}\frac{k_1 c_1}{c_{p1} p_1}\sqrt{2/\gamma}. \tag{35}$$

The non-dimensional equations (23) take the form:

$$0 = f(\bar{u}, \bar{T}), \tag{36a}$$

$$\frac{3}{2M_1}\sqrt{\gamma/2}\,\bar{\mu}\frac{d\bar{T}}{d\bar{x}} = g(\bar{u}, \bar{T}). \tag{36b}$$

The roots of Eq. (36a) are denoted $\bar{u}^{\pm}(\bar{T}) = \frac{1}{2}(\tilde{p}_0 \pm \sqrt{\tilde{p}_0^2 - 4\bar{T}})$ and it can be shown that

$$\bar{u}_1 = \bar{u}^+(\bar{T}_1), \quad \begin{cases} \bar{u}_2 = \bar{u}^+(\bar{T}_2) & \text{if } \gamma M_1^2 < \dfrac{3\gamma - 1}{3 - \gamma}, \\ \bar{u}_2 = \bar{u}^-(\bar{T}_2) & \text{if } \gamma M_1^2 > \dfrac{3\gamma - 1}{3 - \gamma}. \end{cases} \tag{37}$$

There are two possible cases (if $\gamma \geq 1$):

- if $\gamma M_1^2 < (3\gamma - 1)/(3 - \gamma)$ then the integral curve is given by $\bar{u}^+(\bar{T})$ from $(\bar{u}_1, \bar{T}_1)$ to $(\bar{u}_2, \bar{T}_2)$, and the spatial evolution is given by Eq. (36b):

$$\frac{d\bar{x}}{d\bar{T}} = \frac{3}{2M_1}\sqrt{\frac{\gamma}{2}}\frac{\bar{\mu}}{g(\bar{u}, \bar{T})}. \tag{38}$$

- if $\gamma M_1^2 > (3\gamma - 1)/(3 - \gamma)$ then the preceding behavior is still valid from $(\bar{u}_1, \bar{T}_1)$ to $(\bar{u}^+(\bar{T}_2), \bar{T}_2)$, and there is an isothermal jump from $\bar{u}^+(\bar{T}_2)$ to $\bar{u}_2 = \bar{u}^-(\bar{T}_2)$ (without spatial evolution).

This isothermal discontinuity is characteristic of inviscid shocks for Mach numbers larger than 1.34 (for $\gamma = \frac{5}{3}$).

4. A PATH INTEGRATION METHOD BASED ON THE PHASE PLANE ANALYSIS

The methods which may be used to compute the two limit solutions only require some adaptations of the general solution scheme which we briefly describe in this section. Navier–Stokes shock structures can be determined in the phase plane through Eq. (26) using a process described in detail by Hayes [10] and only outlined here. Downstream conditions are first determined from upstream variables, using Rankine–Hugoniot relations (the zeroth order shock relations). The velocity domain is then discretized in N subintervals:

$$\hat{u}_0 = \bar{u}_2, \tag{39a}$$

$$\hat{u}_n = \hat{u}_{n-1} + \delta\hat{u}_n \quad \forall n = 1, ..., N. \tag{39b}$$

A uniform velocity step is adopted except in the immediate neighbourhood of the downstream point:

$$\delta\bar{u} = \frac{\bar{u}_1 - \bar{u}_2}{N - 1}, \tag{40a}$$

$$\delta\hat{u}_1 = \tfrac{1}{100}\,\delta\bar{u}, \tag{40b}$$

$$\delta\hat{u}_2 = \tfrac{99}{100}\,\delta\bar{u}, \tag{40c}$$

$$\delta\hat{u}_n = \delta\bar{u} \quad \forall n = 3, ..., N. \tag{40d}$$

Since the downstream point is a singular point for Eq. (26), the first step from that point must be achieved analytically. It is adequate to use a small increment for this step as specified in Eq. (40b) and progress in the direction of the eigenvector defined by Eq. (34):

$$\hat{T}_0 = \bar{T}_2, \tag{41a}$$

$$\hat{T}_1 = \hat{T}_0 + (\hat{u}_0 - \hat{u}_1)[(2 - \kappa_2^-)\hat{u}_0 - \tilde{p}_0]. \tag{41b}$$

Equation (26) is integrated from thereon according to

$$\hat{T}_{n+1} = \hat{T}_n + \frac{4\,\mathrm{Pr}}{3\gamma}\hat{u}_n\frac{g(\hat{u}_n, \hat{T}_n)}{f(\hat{u}_n, \hat{T}_n)}\delta\hat{u}_{n+1} \quad \forall n = 1, ..., N - 1, \tag{42}$$

and the spatial evolution is given by

$$\hat{x}_0 = 0, \tag{43a}$$

$$\hat{x}_1 = 0, \tag{43b}$$

$$\hat{x}_{n+1} = \hat{x}_n + \frac{4}{3M_1\sqrt{2\gamma}}\frac{\bar{\mu}(\hat{T}_n)\hat{u}_n}{f(\hat{u}_n, \hat{T}_n)}\delta\hat{u}_{n+1} \quad \forall n = 1, ..., N - 1. \tag{43c}$$

Computations have been performed with $N = 101$ subintervals. This number was sufficient to reach the spatial convergence of the solutions. Figure 1 shows the phase plane and

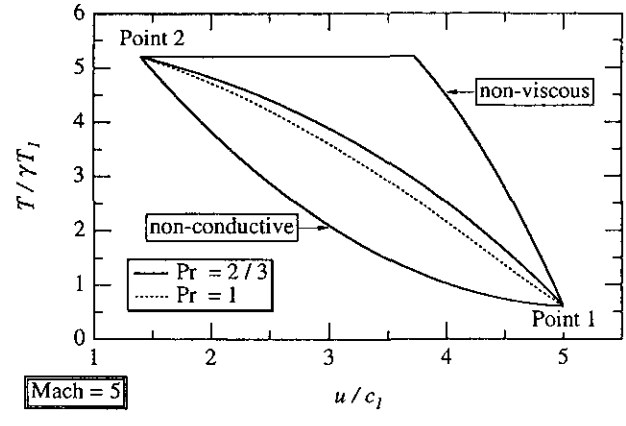

FIG. 1. Representation of the inner shock structure in the phase plane. Variations with the Prandtl number.

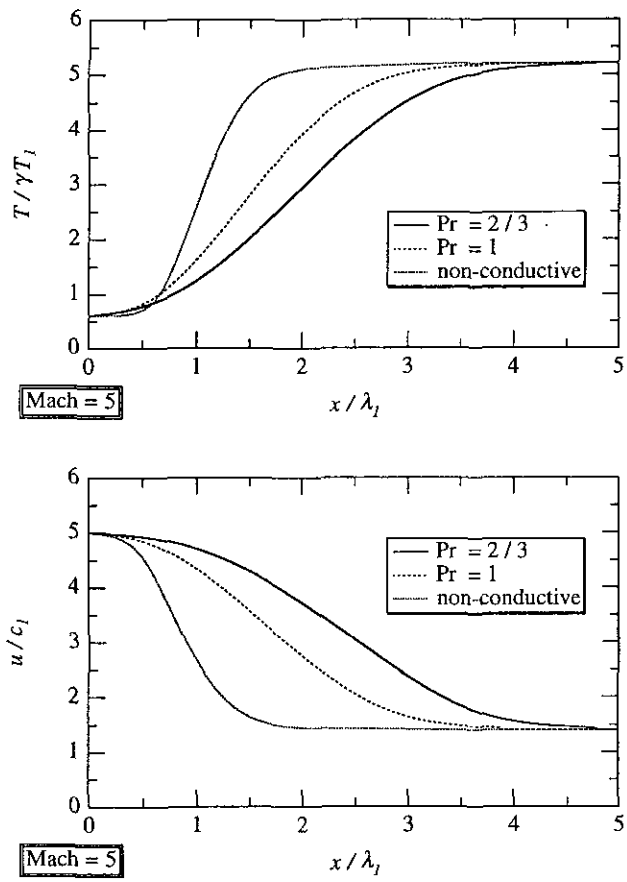

FIG. 2. Spatial evolution of the temperature and velocity in a shock wave, according to the Navier–Stokes equations.

displays the integral curves corresponding to different solutions: the non-conductive case, the non-viscous case, the general cases for Prandtl numbers equal 1 and $\frac{2}{3}$. The last value corresponds to the monatomic gas case. The characteristic features indicated in Section 3 are effectively retrieved:

- the general solutions are limited by the two extreme cases (the non-conductive and the non-viscous);
- the non-viscous solution presents an isothermal jump;
- the integration is performed from point 2 to point 1.

Figure 2 represents the spatial evolution of the temperature and velocity for an upstream Mach number equal to 5. As the Prandtl number increases, the shock becomes steeper because the thermal diffusion is weaker. The shock thickness relative to the upstream mean free path is very sensitive to the Prandtl number.

5. THE FINITE DIFFERENCE GLOBAL SOLUTION METHOD

5.1. *Discretization and Boundary Conditions*

The main difficulty with the previous method is that it is not easily extended to the second-order equations, because the order of the problem precludes a phase plane analysis. While the linear analysis carried out near the downstream point may be used to start the integration, the results obtained exhibit unwanted oscillations (see, e.g., [11]). We propose using a finite difference global solution scheme with well-posed boundary conditions to solve the nonlinear system. This system consists of two ordinary differential equations involving the first and second derivatives of velocity and temperature. Thus two boundary conditions are needed for the velocity, and two for the temperature. It can be noted that there is nothing in the downstream nor in the upstream conditions to fix the location of the shock. In other words, if $[\bar{u}(\bar{x}), \bar{T}(\bar{x})]$ is a solution of the system (23) which converges to the downstream conditions when $\bar{x} \to -\infty$ and to the upstream conditions when $\bar{x} \to +\infty$, then $[\bar{u}(\bar{x}_o + \bar{x}), \bar{T}(\bar{x}_o + \bar{x})]$ is another solution for all real values of $\bar{x}_o$. Hence, to ensure the uniqueness of the solution, another condition must be added and one of the boundary conditions has to be eliminated. Finally, the following conditions are associated with the system (23)

$$\lim_{\bar{x}\to-\infty} \bar{u}(\bar{x}) = \bar{u}_1, \tag{44a}$$

$$\lim_{\bar{x}\to+\infty} \bar{u}(\bar{x}) = \bar{u}_2, \tag{44b}$$

$$\lim_{\bar{x}\to+\infty} \bar{T}(\bar{x}) = \bar{T}_2, \tag{44c}$$

$$\bar{T}(\bar{x}_o) = \tfrac{1}{2}(\bar{T}_1 + \bar{T}_2), \tag{44d}$$

where $\bar{x}_o$ is an arbitrary real value. When considering the Navier–Stokes case, the conditions (44a) and (44c) overdetermine the system (23), since the second-order derivatives of the temperature and velocity are not included in the fluxes; hence, these conditions are removed. This choice is suggested by the phase plane analysis of the Navier–Stokes shock structure and the remark on the uniqueness of the solution.

The spatial domain is chosen to be wide enough to contain the entire shock structure (typically, 30 mean free paths) and it is discretized with a mesh $(\hat{x}_n, n = 1, ..., N)$ which is refined near the center of the domain $\hat{x}_m$, $m = N/2$. The arbitrary real value $\bar{x}_o$ is chosen equal to $\hat{x}_m$.

At the point $\hat{x}_1$, the boundary condition is written

$$\hat{u}_1 - \bar{u}_1 = 0, \tag{45}$$

and Eq. (23b) is discretized using first-order accurate non-centered finite differences:

$$\left(\widehat{\frac{d\bar{s}}{d\bar{x}}}\right)_1 = \frac{\hat{s}_2 - \hat{s}_1}{\hat{x}_2 - \hat{x}_1} \quad \text{for } \bar{s} = \bar{u}, \bar{T}, \tag{46a}$$

$$\left(\widehat{\frac{d^2\bar{u}}{d\bar{x}^2}}\right)_1 = 2\frac{\left(\dfrac{\hat{u}_3 - \hat{u}_1}{\hat{x}_3 - \hat{x}_1} - \dfrac{\hat{u}_2 - \hat{u}_1}{\hat{x}_2 - \hat{x}_1}\right)}{(\hat{x}_3 - \hat{x}_2)}. \tag{46b}$$

At the points $\hat{x}_n$, $n = 2, ..., N-1$, Eqs. (23) are discretized using second-order accurate centered finite differences:

$$\left(\widehat{\frac{d\bar{s}}{d\bar{x}}}\right)_n = \left[(\hat{s}_{n+1} - \hat{s}_n)\frac{\hat{x}_n - \hat{x}_{n-1}}{\hat{x}_{n+1} - \hat{x}_n} + (\hat{s}_n - \hat{s}_{n-1})\frac{\hat{x}_{n+1} - \hat{x}_n}{\hat{x}_n - \hat{x}_{n-1}}\right] \Big/ (\hat{x}_{n+1} - \hat{x}_{n-1}) \quad \text{for } \bar{s} = \bar{u}, \bar{T}, \tag{47a}$$

$$\left(\widehat{\frac{d^2\bar{s}}{d\bar{x}^2}}\right)_n = 2\left[\frac{\hat{s}_{n+1} - \hat{s}_n}{\hat{x}_{n+1} - \hat{x}_n} - \frac{\hat{s}_n - \hat{s}_{n-1}}{\hat{x}_n - \hat{x}_{n-1}}\right] \Big/ (\hat{x}_{n+1} - \hat{x}_{n-1}) \quad \text{for } \bar{s} = \bar{u}, \bar{T}, \tag{47b}$$

except for the point $\hat{x}_m$ for which the temperature equation (23b) is replaced by the relation

$$\hat{T}_m - \tfrac{1}{2}(\bar{T}_1 + \bar{T}_2) = 0. \tag{48}$$

At the point N, the downstream conditions are written

$$\hat{u}_N - \bar{u}_2 = 0, \tag{49a}$$

$$\hat{T}_N - \bar{T}_2 = 0, \tag{49b}$$

except in the Navier–Stokes case, for which the conditions (45) and (49b) are replaced by first-order accurate non-centered finite difference versions of Eqs. (23).

5.2. *Method of Solution*

The set of unknowns may be treated as a vector $\mathbf{U} = (\mathbf{U}_n)^t$, $n = 1, ..., N$, whose elements are 2-component vectors $\mathbf{U}_n = (\hat{u}_n, \hat{T}_n)^t$. The discrete problem consists of solving a non-linear system,

$$\mathbf{F}(\mathbf{U}) = 0, \tag{50}$$

where $\mathbf{F}$ is an N-vector $\mathbf{F} = (\mathbf{F}_n)^t$, $n = 1, ..., N$, whose elements are 2-component vectors $\mathbf{F}_n(\mathbf{U}) = [F_{n1}(\mathbf{U}), F_{n2}(\mathbf{U})]^t$ such that for all $n = 1, ..., N-1$,

$$F_{n1}(\mathbf{U}) = -\frac{1}{M_1\sqrt{2\gamma}}\hat{u}_n\left\{-\frac{4}{3}\bar{\mu}(\hat{T}_n)\left(\widehat{\frac{d\bar{u}}{d\bar{x}}}\right)_n + \frac{2}{3}\frac{\bar{\mu}(\hat{T}_n)^2}{M_1\sqrt{2\gamma}}\frac{\hat{u}_n}{\hat{T}_n}\left[\left(\tilde{\omega}_1 + \frac{1}{3}\tilde{\omega}_6\right)\left(\widehat{\frac{d\bar{u}}{d\bar{x}}}\right)_n^2 + \tilde{\omega}_3\left(\widehat{\frac{d^2\bar{T}}{d\bar{x}^2}}\right)_n + \frac{\tilde{\omega}_5}{\hat{T}_n}\left(\widehat{\frac{d\bar{T}}{d\bar{x}}}\right)_n^2\right]\right\} - \hat{T}_n - \hat{u}_n^2 + \hat{p}_0\hat{u}_n, \tag{51a}$$

$$F_{n2}(\mathbf{U}) = -\frac{1}{\mathrm{Pr}\,M_1}\sqrt{\gamma/2}\left\{-\bar{\mu}(\hat{T}_n)\left(\widehat{\frac{d\bar{T}}{d\bar{x}}}\right)_n + \frac{\gamma-1}{\gamma}\frac{\mathrm{Pr}\,\bar{\mu}(\hat{T}_n)^2}{M_1\sqrt{2\gamma}}\frac{\hat{u}_n}{\hat{T}_n}\left[\left(\theta_1 - \frac{5}{3}\theta_2 + 2\theta_5\right)\left(\widehat{\frac{d\bar{u}}{d\bar{x}}}\right)_n\left(\widehat{\frac{d\bar{T}}{d\bar{x}}}\right)_n - \frac{2}{3}\theta_2\hat{T}_n\left(\widehat{\frac{d^2\bar{u}}{d\bar{x}^2}}\right)_n\right]\right\} - \hat{T}_n + \frac{\gamma-1}{2}\hat{u}_n^2 - (\gamma-1)\tilde{p}_0\hat{u}_n + \tilde{h}_0, \tag{51b}$$

except for $n = m$, for which

$$F_{m2}(\mathbf{U}) = \hat{T}_m - \tfrac{1}{2}(\bar{T}_1 + \bar{T}_2) \tag{52}$$

and

$$F_{11}(\mathbf{U}) = \hat{u}_1 - \bar{u}_1, \tag{53a}$$

$$F_{N1}(\mathbf{U}) = \hat{u}_N - \bar{u}_2, \tag{53b}$$

$$F_{N2}(\mathbf{U}) = \hat{T}_N - \bar{T}_2. \tag{53c}$$

In the Navier–Stokes case, Eq. (51a) is retained at the upstream end, instead of (53a), and Eq. (51b) is retained at the downstream end, instead of (53c).

This system is solved in an iterative manner by the Newton method. The jacobian of the non-linear function $\mathbf{F}$ is evaluated numerically. If the dependences of $(\widehat{d^2\bar{T}/d^2\bar{x}})_1$ and $(\widehat{d^2\bar{T}/d^2\bar{x}})_N$, respectively, on $\hat{T}_3$ and $\hat{T}_{N-2}$ are neglected (and similarly for the second derivative of the velocity), the jacobian has the form of a tridiagonal $N \times N$ matrix whose elements are 2×2 blocks. Starting from an initial set of values $\mathbf{U}^o = (\hat{u}^o, \hat{T}^o)^t$, the following system has to be solved at each Newton step,

$$\frac{d\mathbf{F}}{d\mathbf{U}}(\mathbf{U}^i)(\mathbf{U}^{i+1} - \mathbf{U}^i) = -\mathbf{F}(\mathbf{U}^i), \tag{54}$$

until the L_2 norm of $\mathbf{F}$ is small enough. Each block of the jacobian is inverted directly, and a recursive algorithm is used to solve the tridiagonal system (54).

The initial solution consists of hyperbolic tangent profiles for $\hat{u}^o$ and $\hat{T}^o$, connecting the upstream and downstream conditions. The mesh is adapted to obtain constant jumps in velocity between two successive points. This is done with the profiles

$$\hat{u}_n^o = \bar{u}_1 + (n-1)\frac{\bar{u}_2 - \bar{u}_1}{N-1}, \tag{55a}$$

$$\hat{T}_n^o = \bar{T}_1 + (n-1)\frac{\bar{T}_2 - \bar{T}_1}{N-1} \tag{55b}$$

for all $n = 1, ..., N$, on the mesh defined as

$$\hat{x}_n = \frac{1}{2}(\hat{x}_1 + \hat{x}_N) + \frac{1}{2}\frac{\hat{x}_N - \hat{x}_1}{\operatorname{argth}\dfrac{1}{1+\lambda}} \operatorname{argth}\left[\frac{2\hat{u}_n^o - (\bar{u}_1 + \bar{u}_2)}{(1+\lambda)(\bar{u}_2 - \bar{u}_1)}\right], \tag{56}$$

with $\hat{x}_1 = 0$, $\hat{x}_N = 30$, and $\lambda = 5 \times 10^{-2}$.

6. RESULTS AND DISCUSSION

6.1. *Validation in the Navier–Stokes Case*

It is first appropriate to test the FDGS scheme in the Navier–Stokes case. As the governing equations (25) are only first-order, two boundary conditions must be eliminated. The conditions (44a) and (44c) on the upstream velocity and the downstream temperature are replaced by the appropriate non-centered discretized versions of the first-order equations. One finds that only 10 iterations are needed for the Newton method to decrease the L_2 norm of the residuals by 10 orders of magnitude. The spatial convergence is reached with $N = 101$ mesh points.

Studies of shock structure are generally validated by comparing the reciprocal density thickness with experimental measurements. This thickness is conventionally defined as

$$L = (\rho_2 - \rho_1) \Big/ \left(\frac{d\rho}{dx}\right)_{\max} \tag{57}$$

Figure 5 displays the results concerning the reciprocal density thickness. It compares the solutions of the path integration and FDGS methods and also shows experimental measurements [12]. The first conclusion is that both methods give very close results for the Navier–Stokes shock structure. The test confirms the validity of the FDGS scheme with the boundary conditions indicated above. The second conclusion is that the Navier–Stokes results differ significantly from the experimental measurements for Mach numbers larger than about 1.5. This only confirms that the first-order Navier–Stokes fluxes do not adequately describe the inner shock wave structure. Second-order equations are needed, as is shown in the next subsection.

6.2. *The Second-Order Results*

The method described in Section 5 is now applied to the second-order equations (23), as described by Eqs. (51)–(54). As for the Navier–Stokes equations, convergence is reached within 10 Newton iterations. For Mach numbers larger than 8, the computation must be initialized with an extrapolation of the solution obtained at smaller Mach numbers. If care is taken over this, the calculation remains quite easy, even for large values of the Mach number (computations have been performed up to a Mach number of 30). Solutions obtained for upstream Mach numbers equal to 5 and 10 are plotted in Figs. 3 and 4. They show that the Woods second-order theory predicts thicker shock waves than those determined from the Navier–Stokes equations.

As was expected, the shock profiles show some oscillations at the downstream end, mainly in the temperature profile. These oscillations are independent of mesh size and discretization, and so they must be regarded as part of the solution of the second-order equations. They amount to some 3–4% of the magnitude of the total difference between upstream and downstream temperature, but considerably less for the velocity profile. At the far downstream, the oscillations decrease in magnitude until the stationary state is reached. Experimental work does not report these oscillations; however, the experimental data is accurate to within 1–2% (see [12]) and may not be tuned to identify downstream oscillations in the temperature. Other researchers in numerical gas dynamics report these oscillations in Monte Carlo direct simulations of the monatomic gas shock profile, although they have a smaller magnitude (see, e.g., [13]). The Monte Carlo simulations are assumed to accurately model gas dynamics in the hypersonic regime we are interested

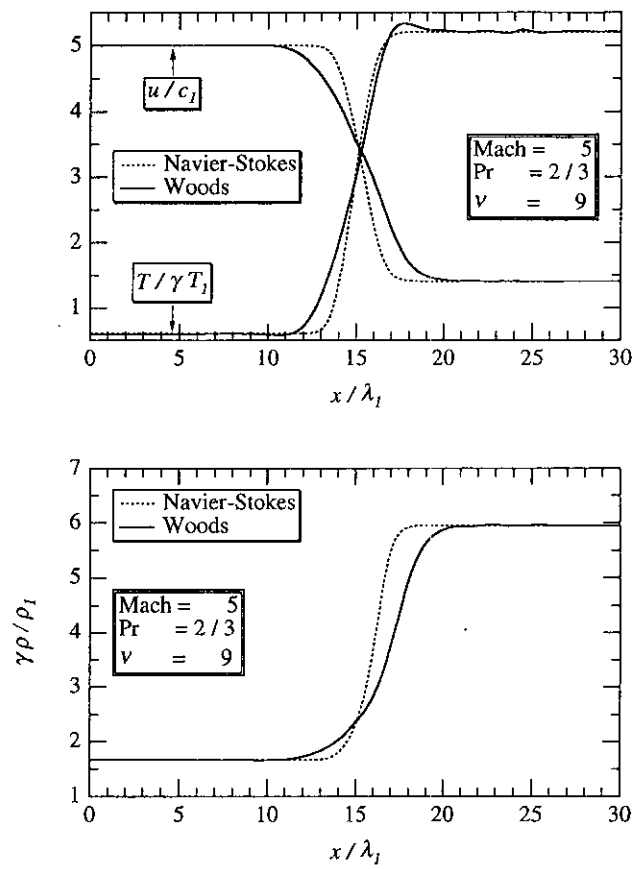

FIG. 3. Comparison of the first- and second-order shock structures for an upstream Mach number equal to 5. The solutions are obtained with the FDGS method.

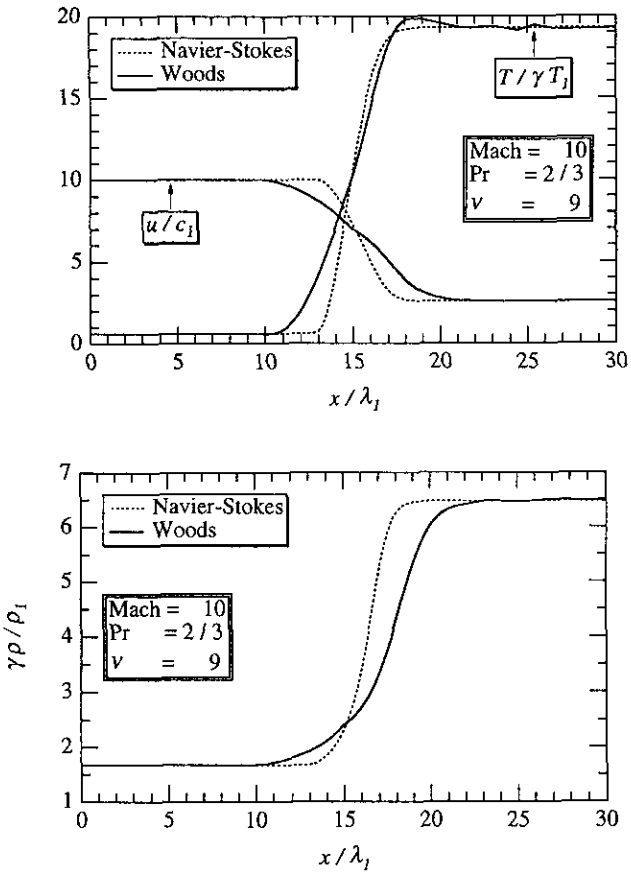

FIG. 4. Comparison of the first- and second-order shock structures for an upstream Mach number equal to 10. The solutions are obtained with the FDGS method.

in; however it is, at present, unknown what physical effect gives rise to these oscillations.

As shown in Fig. 5, the shock reciprocal density thickness is very close to the experimental measurements up to the Mach number where measurements are available (Mach 10). Above this limit our solution follows the experimental trend (Fig. 5). The results obtained in this case demonstrate that the Woods formulation as defined in this article constitutes a useful second-order expansion.

One may ask if it is possible to define a model which would not exhibit slight oscillations. An eigenvalue analysis of the fluxes (17) indicates that the sources of oscillations in the shock solution are the second-order derivatives. To understand this effect in physical terms one may consider the one-dimensional steady energy equation including the flux:

$$q_{sW}^{(2)} = R\frac{\mu^2}{p}\left[(\theta_1 + 2\theta_5)\frac{du}{dx}\frac{dT}{dx} + \theta_2 u\frac{d^2T}{dx^2}\right]. \qquad (58)$$

This flux is obtained from (17b), where the second-order derivative of the velocity is replaced by the second-order derivative of the temperature through the steady form of the Euler conservation equation (15b). The second-order derivative of the temperature gives rise to a third-order term in the energy equation which takes a form analogous to the Korteweg–de Vries equation. Now, it is known that the KdV equation exhibits shock profiles modulated by oscillations (see, e.g., [8]). This behavior is avoided by taking $\hat{\omega}_3 = 0$ and $\theta_2 = 0$ as confirmed by systematic calculations with various forms of the second-order fluxes. Monotonic solutions are obtained when the second-order fluxes are specified in this way. This is exemplified in Fig. 6. The reciprocal density thickness calculated with the simplified second-order fluxes is displayed in Fig. 5 with the label "simplified Woods." The results are as good as those of the complete Woods formulation but the theoretical foundation of the simplified fluxes is less firmly based. This analysis indicates that: (1) the second-order derivatives are responsible for the oscillations in the shock solution; (2) these terms only weakly influence the shock wave structure, and they may be neglected if one wishes to obtain oscillation free shock profiles. For practical purposes (like for full three-dimensional rarefied gas numerical calculations), one would get nearly the same results without the difficult second-order derivative terms. It is expected that

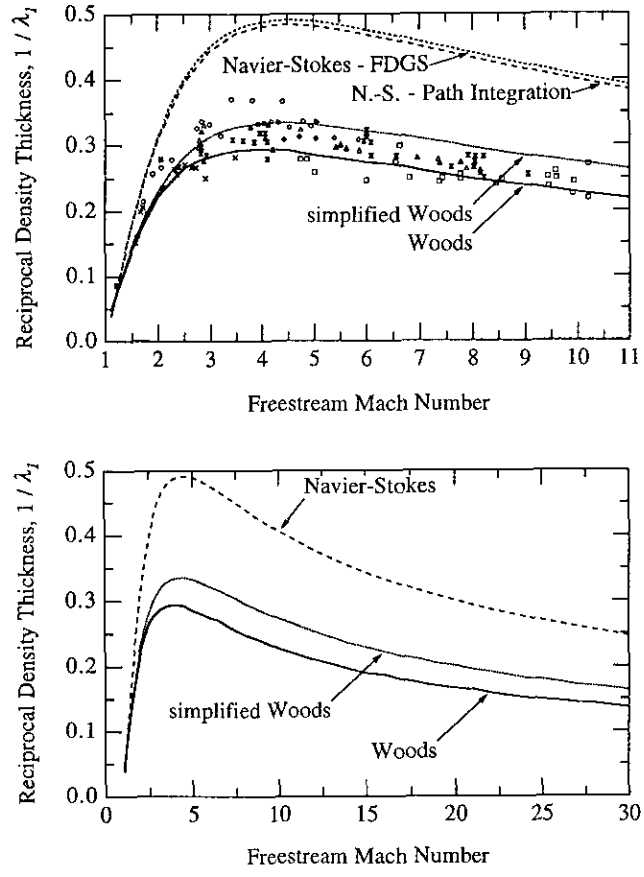

FIG. 5. Shock reciprocal density thickness versus the upstream Mach number. The experimental data are taken from [12].

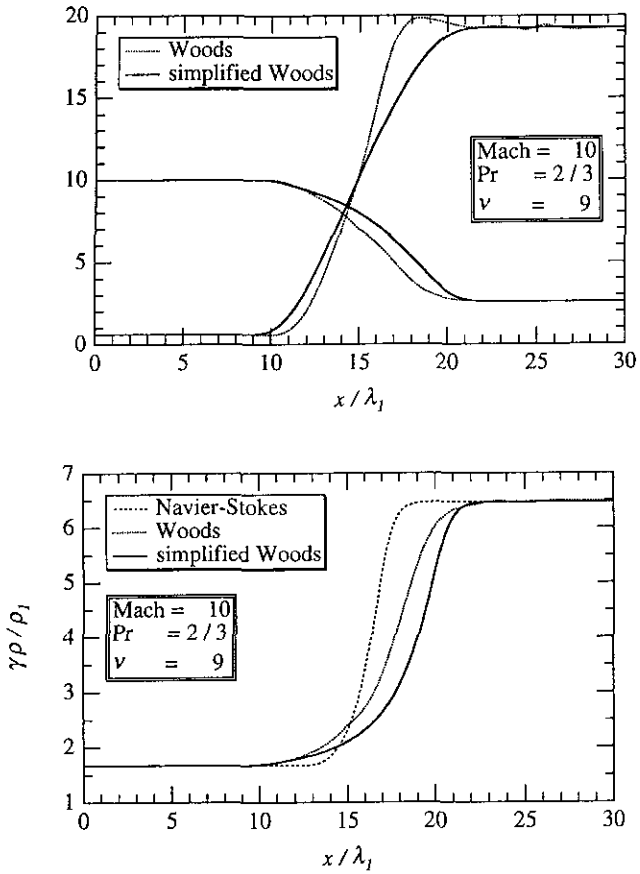

FIG. 6. Shock wave structure as described by the simplified Woods fluxes, compared to the results obtained with the complete Woods fluxes at Mach 10.

the simplified fluxes will pose fewer numerical problems. These forms may be recommended on these grounds and also because they are easier to implement.

7. CONCLUSIONS

A second-order theory is used to describe shock wave structures. The equations obtained are solved with a finite difference global scheme which has not previously been used for this type of problem. A set of simplified second-order fluxes is also devised and recommended for three-dimensional numerical calculations of hypersonic flows in the continuum transitional regime. The results obtained in one dimension with the exact and simplified fluxes are close to the experimental measurements of the shock thickness in a monatomic gas for upstream Mach numbers below 10. Beyond this value no experimental data exists as yet, but a good theoretical trend is obtained. The extension to a diatomic gas is quite easy, but much more theoretical effort must be expended to deal with reacting mixtures.

ACKNOWLEDGMENTS

The authors wish to thank the reviewers of the early drafts of this paper for their many helpful comments.

REFERENCES

1. S. Chapman and T. G. Cowling, *The Mathematical Theory of Non-Uniform Gases*, 3rd ed. (Cambridge Univ. Press, Cambridge, 1970).
2. L. C. Woods, *An Introduction to the Kinetic Theory of Gases and Magnetoplasmas* (Oxford Univ. Press, Oxford, 1993).
3. F. J. P. Thivet, S. M. Candel, and M.-Y. Perrin, in *Proceedings, 1st Intl. Symp. on the Aerothermodynamics of Space Vehicles, Noordwijk, The Netherlands*, ESA SP-318, p. 325.
4. M. D. Smooke, *J. Comput. Phys.* **48,** 72 (1982).
5. F. E. Lumpkin and D. R. Chapman, AIAA Paper 91-0771, 1991 (unpublished).
6. X. Zhong, R. W. MacCormack, and D. R. Chapman, AIAA Paper 91-0770, 1991 (unpublished).
7. W. T. Welder, D. R. Chapman, and R. W. MacCormack, AIAA Paper 93-3094, 1993 (unpublished).
8. V. I. Karpman, *Non-linear Waves in Dispersive Media* (Pergamon, Oxford, 1975), p. 101.
9. G. S. S. Ludford, *J. Aeronaut. Sci.* **18,** 830 (1951).
10. W. D. Hayes, "The Basic Theory of Gasdynamic Discontinuities," in *High Speed Aerodynamics and Jet Propulsion, Volume III: Fundamentals of Gas Dynamics*, edited by H. W. Emmons (Princeton Univ. Press, Princeton, NJ, 1958), p. 416.
11. F. S. Sherman and L. Talbot, in *Proceedings, 1st Intl. Symp. on Rarefied Gas Dynamics*, edited by F. M. Devienne (Pergamon, New York, 1960), p. 161.
12. H. Alsmeyer, *J. Fluid Mech.* **74,** 497 (1976).
13. E. Salomons and M. Mareschal, *Phys. Rev. Lett.* **69,** 269 (1992).